2
Materials and Methods

In vitro analysis of organophosphate pesticide (OP)-protein interaction is, in general, accomplished by employing a combination of biophysical techniques. This Chapter includes a detailed description of various experimental methods and molecular docking used during the research work described in the current thesis. Special emphasis has been provided for solution-state ^{1}H Nuclear Magnetic Resonance (NMR) based methods.

2.1 MATERIALS USED

Bovine Serum Albumin (BSA) (98% purity, nuclease, and protease-free) was purchased from Hi-Media Laboratories Pvt Ltd., Mumbai, India, while all other chemicals were procured from Sigma-Aldrich Chemicals Pvt Ltd., Bangalore, India and used without any further purification. All reagents were of analytical grade. Double distilled water was used throughout the experiments. Samples of organophosphate pesticides (OP) and their metabolites were prepared within an isolated chamber, considering the safety issues. The description of chemicals is given in Table 2.1.

Table 2.1 : Description of chemicals used in the current thesis.

Chemicals	**Description**	**Molecular Weight**
BSA	Bovine Serum Albumin	66.5 KDa
Trypsin	Trypsin (Porcine Pancreas)	23.3 KDa
Chlorpyrifos	*O*, *O*-Diethyl *O*-3,5,6-trichloropyridin-2-yl phosphorothioate	350.59 g/mol
Diazinon	O, O-Diethyl O-[4-methyl-6-(propan-2-yl) pyrimidin-2-yl] phosphorothioate	304.34 g/mol
Parathion	*O*, *O*-Diethyl *O*-(4-nitrophenyl) phosphorothioate	291.26 g/mol
TCPy	3,5,6-Trichloro-1*H*-pyridin-2-one	198.43 g/mol
IMP	2-isopropyl-6-methyl-pyrimidin-4-ol	152.19 g/mol
Paraoxon Methyl	*O*, *O*-Dimethyl *O*-(4-nitrophenyl) phosphate	247.14 g/mol
Warfarin	4-hydroxy-3-(3-oxo-1-phenylbutyl) chromen-2-one	308.33 g/mol

Ibuprofen	2-[4-(2-methylpropyl) phenyl]propanoic acid	206.29 g/mol
Diapotassium Phosphate	Potassium hydrogenphosphate Potassium hydrogen(tetraoxidophosphate) (2−)	174.2 g/mol
Monopotassium Phosphate	Potassium dihydrogenphosphate Potassium dihydrogen(tetraoxidophosphate) (1−)	136.086 g/mol
Deuterated Solvents	DMSO d_6 and D_2O	
BAEE	N_α-Benzoyl-L-arginine ethyl ester hydrochloride (BAEE)	342.82

2.2 SAMPLE PREPARATION

The phosphate buffer (PB) of pH 7.4±0.05 was used for protein samples preparation throughout the thesis using monopotassium phosphate and dipotassium phosphate. The stock solutions of protein samples were prepared in PB and ligands stocks were prepared in the solvent combination of D_2O: DMSO, due to the low solubility of test ligands in water.

2.3 NMR EXPERIMENTS USED FOR OP-PROTEIN INTERACTION STUDY

All the NMR spectra were recorded on a Bruker Ascend 500 MHz Wide Bore (WB) NMR spectrometer equipped with a BBFO probe head. Chemical shifts were referenced to the residual solvent signal of HDO at 4.69 ppm. As described in Chapter 1, there are number of powerful solution-state NMR experiments reported in the literature to study ligand-protein interactions [Cala et al, 2014a; Fielding, 2003, 2007; Ludwig, 2009; Nitsche and Otting, 2018; Unione et al, 2014]. In the present thesis, both qualitative and quantitative NMR experiments based on ^1H chemical shifts and linewidth, spin-lattice relaxation, and Nuclear Overhauser Enhancement (NOE) measurements were performed. A basic introduction to solvent suppression techniques used for these experiments has been given in section 2.3.1, followed by a detailed description of each of these NMR methods.

2.3.1 Solvent Suppression Techniques for Aqueous Ligand-Protein Solutions

Acquiring ^1H NMR spectrum of an aqueous ligand-protein solution exhibiting measurable ligand intensity is challenged by the presence of a huge residual water signal. To overcome this situation, several solvent suppression techniques have been proposed in the literature [Parella, 2006]. The solvent suppression technique is useful for samples where the solvent signal overshadows the analyte intensity. The various solvent suppression techniques employed in literature use selective saturation of the unwanted solvent signal. Both single and multi-selective approaches are proposed [Liu et al, 1998; Parella et al, 1998; Smallcombe et al, 1995; Stott et al, 1995]. Figure 2.1 shows a representative set of pulse programs used for routine solvent suppression using either continuous wave (CW) radiofrequency (RF) pulse or selective shaped pulse or gradient-based composite pulse scheme for the solvent peaks. These solvent suppression methods are capable of suppressing more than one solvent peaks. In the present thesis standard Bruker solvent suppression pulse schemes are used.

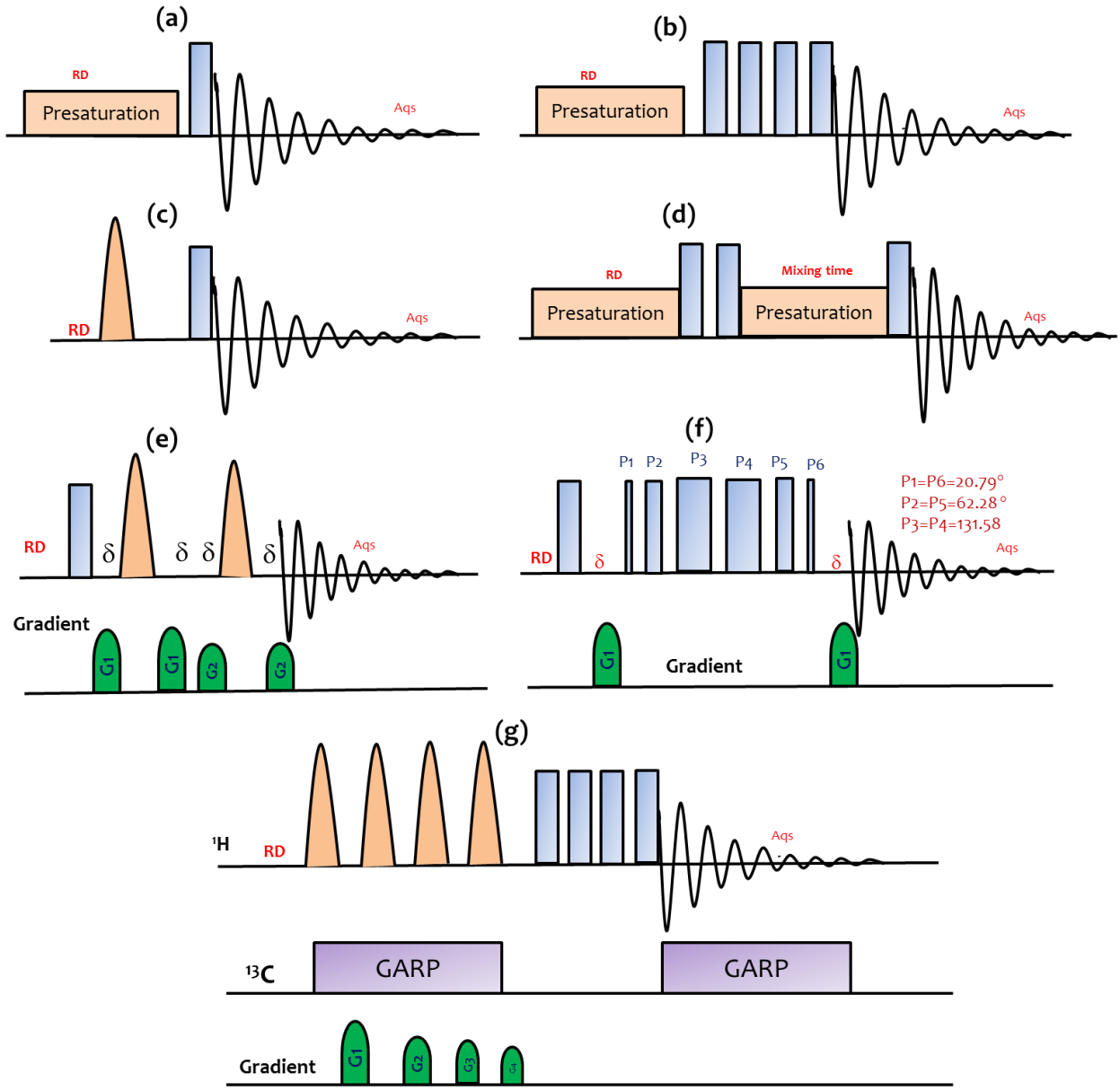

Figure 2.1 : Schematic drawing of different solvent presaturation pulse sequences: (a) conventional pulse (zgpr), (b) composite pulse (zgcppr), (c) shaped pulse (zgps), (d) noesy sequence (noesypr1d), (e) Excitation sculpting (zgesgp), (f) WATERGATE (p3919gp), (g) WET scheme (wet). RD: relaxation delay; Aqs: acquisition time; retangular blue bar: hard 90°, Brown Guassian shaped pulse: selective 180° pulse; green bars: gradient pulses.

The solvent presaturation with conventional pulse sequence (zgpr) can be achieved by keeping the transmitter frequency of a long narrow, low power (mW) continuous wave RF pulse with pulse duration in seconds at the chemical shift position of the solvent signal during the relaxation delay (before the pulse sequence). It saturates the solvent resonance at the transmitter frequency. On the other hand, in the case of composite pulses (zgcppr), the long narrow pulse is usually followed by a rapid succession of four 90° pulses to reduce the residual hump of the water signal. Further, for the solvent presaturation using shaped pulse for the off-resonance (zgps) scheme, the transmitter frequency of the shaped selective pulse is placed at the chemical shift of the solvent signal during the relaxation delay. The limitation of these methods is that they significantly reduce the intensity of exchangeable protons along with solvent peak suppression. Due to this reason, other schemes such as WATERGATE [Piotto et al, 1992], WET [Smallcombe et al., 1995], and Excitation Sculpting [Warren & Pines, 1982] should be preferred in case of

exchanging systems. For the present thesis, excitation sculpting has been used to achieve the multiple solvent suppression for a mixture of solvents. The excitation sculpting, also known as Double Pulsed-Field-Gradient Echo (DPFGE) scheme uses a double echo experiment with a selective 180° pulse [Jerschow & Müller, 1997]. The selective 180° pulse flanked by two gradients ensures the refocusing of only selected resonances at the end of the echo. It can be easily incorporated in the 2D, 3D, and 4D homo and heteronuclear NMR experiments without further requirement of any phase cycling. Different shaped pulses are available to suppress the solvent peak and need to be calibrated according to experimental requirement [Ley et al, 2014].

Figure 2.2 (A) shows the implementation of the solvent suppression techniques on single solvent peak suppression. Multiple solvent suppression technique is required for a mixture of solvents. Double solvent suppression for mixture of two solvents is achieved by using zgps, and excitation sculpting with phase modulation according to offset frequencies, as shown in Figure 2.2 (B). In the current thesis, zgps, and excitation sculpting are used for single solvent suppression, whereas for double solvent suppression (mixture of solvent) excitation sculpting for STD NMR and zgps for relaxation study are employed with phase modulation.

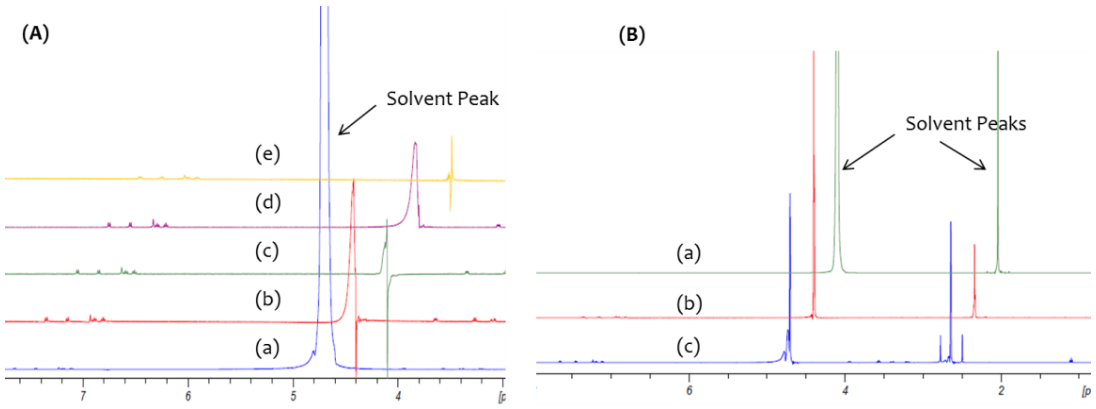

Figure 2.2 : ^{1}H NMR spectrum for tryptophan to show the efficiency of different solvent suppression pulse sequences. (A) (a) zg (without solvent presaturation), (b) zgpr, (c) zgcppr, (d) zgps, (e) excitation sculpting for single solvent suppression and (B) (a) zg, (b) excitation sculpting, and (c) zgps for double solvent suppression.

2.3.2 Chemical shift and line width change (line-broadening and signal intensity loss)

The proton chemical shift is sensitive to the chemical environment as well as intermolecular interactions between ligand-protein systems. Change in the chemical environment due to complexation or due to intermolecular interaction with neighbors in solution will be reflected as a shift either to the higher frequency (downfield) or to the low frequency (upfield) depending on the magnetic shielding properties of the new environment. Besides changes in the NMR chemical shift, the mobility of the molecule also exhibits drastic changes due to the complexation or formation of intermolecular adducts. NMR spectral line of a small molecule in solution at room temperature is in general sharp while that of a macromolecule is broad. This is due to the difference in their correlation time (τ_c) in solution, which is governed by the molecular weight of the chemical species. Complex formation with the protein leads to a more macromolecule like behavior for the small molecule *viz*., a decrease in molecular motion and an increase in molecular correlation time (τ_c) [Cala et al,2014b; Fielding, 2003; Ludwig and Guenther, 2009]. Consequently, a cumulative effect of complexation is observed as NMR line broadening, revealing a much smaller transverse relaxation time (T_2) of the bound small molecule.

The apparent transverse relaxation time (T_2^*) that determines the line width is a direct manifestation of the correlation time. Eq.(2.1) depicts the relation between line width and apparent T_2^*.

$$\Delta\nu_{1/2} = \frac{1}{\pi T_2^*} \tag{2.1}$$

where $\Delta\nu_{1/2}$= observed line width at half height.

Hence any change in the molecular weight due to the complexation can be identified by analyzing the changes observed in the line width of the molecule. The example for the same is shown in Figure 2.3, where *in vitro* ligand detected ^{1}H NMR methods based on the change in the chemical shift, and the line width has been employed to experimentally confirm the interaction of tyrosine phosphatases and HRAS with biotin [Salian et al, 2019]. Figure 2.3 represents a stack plot of the relevant spectral regions of biotin, a small molecule in the free state, and in the presence of protein. Table 2.2 documents the ^{1}H NMR chemical shift, line width and apparent transverse relaxation time for all the peaks of biotin in the free as well as in the bound state.

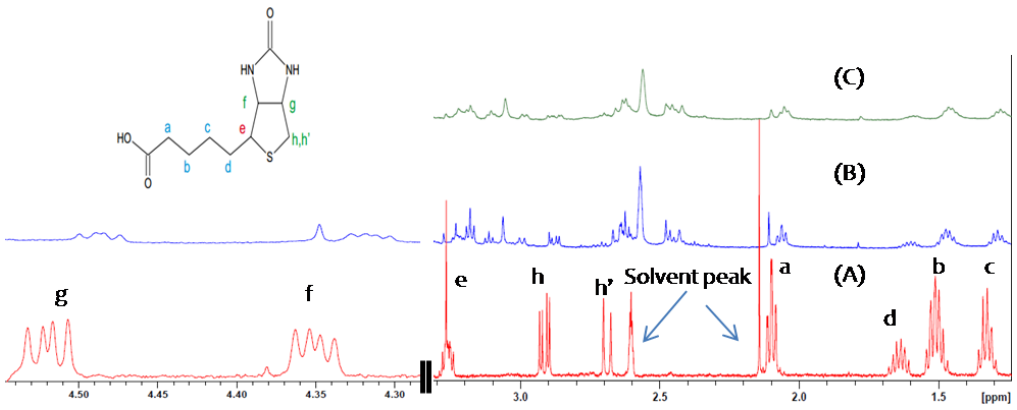

Figure 2.3 : ^{1}H NMR spectral region (A) free Biotin (red spectra) (B) biotin in the presence of tyrosine phosphatases (blue) (C) biotin in the presence of HRAS recorded in tris-HCl buffer (10% DMSO) at 300 K. The area from 4.30-4.6 ppm for free biotin and biotin in the presence of tyrosine phosphatases has been magnified while the same for the HRAS is not shown due to phase distortion in biotin peaks in this area.

A close inspection of Figure 2.3 reveals an upfield shift of all the chemical shifts of biotin in the presence of both the proteins indicating complex formation causing magnetic shielding of the biotin protons. The chemical shift change ($\Delta\delta$) for biotin protons in the free and bound state estimated from the data shown in Table 2.2 exhibits variations from 0.03 to 0.05 ppm in both the cases. Furthermore, due to the formation of the biotin-protein complex undergoing a continuous exchange between free and bound state, a significant change in transverse relaxation times of all the biotin protons is observed. According to Table 2.2, in the case of tyrosine phosphatases, the maximum change in apparent transverse relaxation time is 61.4% for H_e of biotin, whereas for HRAS, the change for the same proton is 89%. In the case of HRAS, the maximum change observed is 91.6% for H_d proton. On average, the change in T_2^* in the presence of tyrosine phosphatases, and HRAS is 29.31% and 72.95%, respectively. These results seem to be indicating that the biotin-HRAS interaction is stronger than biotin-tyrosine phosphatases. However, it must be noted that quantification of the complexation process cannot be achieved through such analysis of linewidth and chemical shift changes. These NMR parameters can, therefore, be used only for preliminary confirmation of molecular interaction between the small ligand and the protein.

Table 2.2 : Chemical shift and line width values of biotin protons in the absence and presence of the protein tyrosine phosphatases and HRAS. #LB is 1Hz in each case.

	Free Biotin protons			Biotin-tyrosine phosphatases			Biotin-HRAS		
Proton Position	**Chemical shift (ppm)**	**Line-width # (Hz)**	**T_2^*(s)**	**Chemical shift (ppm)**	**Line-width (Hz)**	**T_2^*(s)**	**Chemical shift (ppm)**	**Line-width (Hz)**	**T_2^*(s)**
H_c	1.33	3.90	0.081	1.29	4.56	0.069	1.28	5.37	0.059
H_b	1.51	4.46	0.071	1.47	6.94	0.045	1.46	24.68	0.012
H_d	1.64	3.30	0.096	1.61	4.95	0.064	1.59	39.28	0.008
H_a	2.09	3.47	0.091	2.06	3.89	0.081	2.05	7.25	0.043
$H_{h'}$	2.69	2.18	0.146	2.64	2.49	0.127	2.63	7.52	0.042
H_h	2.91	1.27	0.250	2.88	1.87	0.170	2.87	5.31	0.059
H_e	3.26	1.51	0.210	3.23	3.92	0.081	3.22	13.46	0.023
H_f	4.52	2.07	0.153	4.48	3.19	0.099	4.47	13.41	0.023
H_g	4.35	2.90	0.109	4.32	3.98	0.080	4.31	14.99	0.021

In the following sections, two quantitative ligand-based NMR methods employing NMR Magnetization Transfer (MT) and spin-lattice relaxation analysis have been discussed in detail to highlight the popularity and applicability of such NMR methods for quantitation of ligand-protein complexation process.

2.3.3 Saturation Transfer Difference NMR

Saturation Transfer Difference (STD) NMR represents one of the most sensitive experimental method employed to screen ligand libraries with binding affinity in the mM-μM range that allows probing binding interaction of unlabeled protein used in minimal quantity [Bernd Meyer & Peters, 2003b]. The most prominent advantage of STD NMR is that it helps in Group Epitope Mapping (GEM) of a ligand (by proton signals intensity as more intense ligand's signals are in close contact with protein) besides quantifying the binding affinity. GEM, through STD NMR, offers the structural details of these interactions [Angulo et al, 2010,Cala and Krimm, 2015,Gairí et al, 2016,Krishnan, 2005, Mayer and Meyer, 2001,Wagstaff et al, 2013]. Further, binding can be used for the screening of ligands in a mixture of molecules [M. Mayer & Meyer, 2001]. The limitation of routine STD NMR is that it does not reveal any information about the protein's amino acid residues contacting the ligand. Monaco et al, 2017 reports the differential epitope mapping by STD NMR (DEEP-STD NMR) that is capable of providing information about protein residues that are in close proximity with the ligand [Monaco et al, 2017]. Wagstaf et al, 2013 discusses the advantages and disadvantages of several STD NMR methods that people are using for routine STD NMR analysis [Wagstaff et al, 2013b].

STD NMR method is one of the most efficient ligand-based NMR techniques working on the principle of Nuclear Overhauser Enhancement (NOE) employed to analyze ligand binding with protein. In STD NMR, the macromolecule NMR resonances are selectively saturated by applying radio-frequency irradiation. The saturation can then propagate along the macromolecule length via intramolecular spin-diffusion. Further, the effect of saturation is transferred to the ligand due to intermolecular dipolar interaction between ligand-protein during association/complexation. STD NMR spectrum is thus recorded by acquiring two consecutive experiments, namely the off-resonance STD (STD_{off}) experiment, and the on-resonance STD (STD_{on}) version. The STD_{off} is recorded either without protein saturation, or with the saturation pulse applied far away from protein resonances, whereas the STD_{on} resonance spectrum is acquired by selectively irradiating at a region that contains only receptor resonances [Angulo and Nieto, 2011,Cala et al., 2014, Mayer and Meyer, 2001]. Finally, the desired STD spectrum (STD_{Diff}) is obtained by subtracting the on-resonance spectrum (STD_{on}) from the off-resonance spectrum (STD_{off}). The ligand molecules that are spatially proximal with the macromolecule receive the highest saturation transfer and exhibit the most intense STD signals in the STD_{Diff} spectrum. Resonances observed in the STD_{Diff} spectrum are, in general, appear with varying intensities indicating the variable amount of saturation transfer received by the ligand nuclei based on their spatial distance from the protein. Ligand nuclei that are far from the protein will not appear in the difference spectrum, as illustrated in Figure 2.4. In 1999, Mayer and Meyer used the STD NMR to reveal ligand-receptor binding.

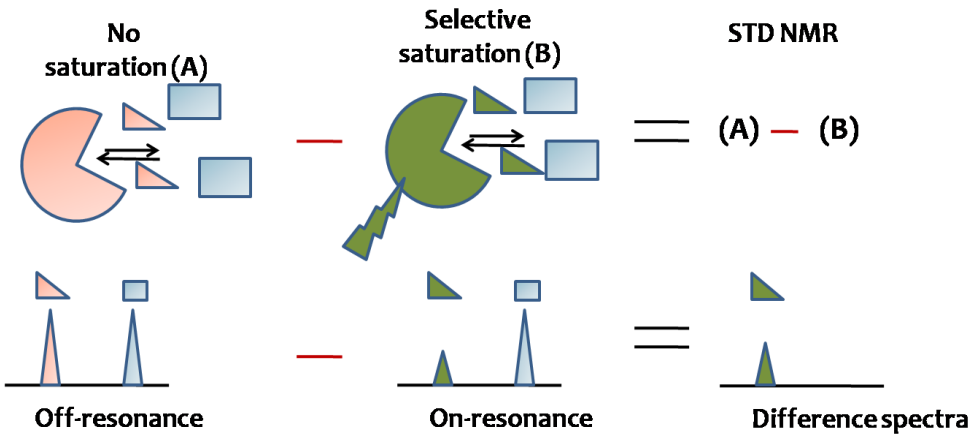

Figure 2.4 : STD NMR Mechanism (A) off-resonance spectrum (B) on-resonance spectrum (C) Difference spectrum where only bound ligand resonance is observed [Mayer and Meyer, 1999; Meyer and Peters, 2003a].

The pulse sequence for STD NMR used in the current thesis is a standard Bruker pulse sequence with solvent suppression (Figure 2.5). The protein saturation is acquired by a selective Gaussian pulse because the use of a Gaussian pulse reduces the problem of side-bands and uniformly excites the selected region. For STD NMR experiments, the ligand to protein ratio can vary from 20:1 to 100:1. The irradiation of protein is performed in the area of -3 to 1 ppm (valine, leucine, and isoleucine residues), where no ligand signals appear or in the area of the aromatic region 6-8 ppm. The intensity of STD signals depend on the saturation time (duration of RF irradiation of the protein).

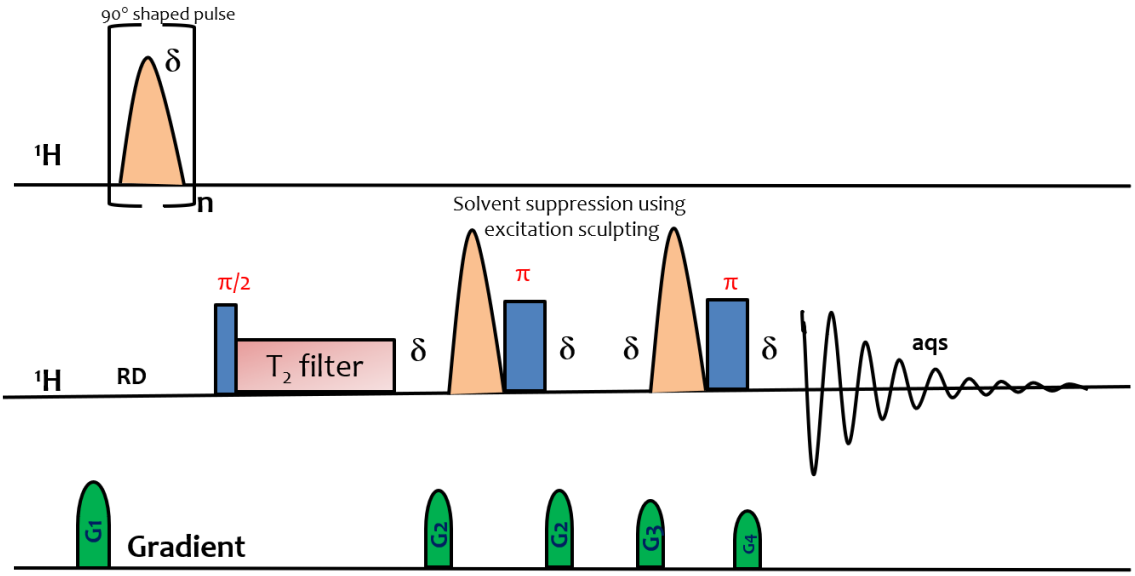

Figure 2.5 : Conventional STD NMR pulse sequence with excitation sculpting [Mayer and Meyer, 2001]. RD: relaxation delay; Aqs: acquisition time; retangular blue bar: hard pulses, Brown Guassian shaped pulse: selective 180° pulse; green bars: gradient pulses

For quantification of the transfer of saturation from the protein to the ligand during association, integrals of spectral lines observed in the STD_{diff} spectrum are required. These set of line integrals are designated as I_{STD} and defined by Eq.(2.2) [Meyer and Peters, 2003b]:

$$I_{STD} = \frac{I_o - I_{sat}}{I_o} \tag{2.2}$$

where I_o is the intensity of the reference spectrum, and I_{sat} is the intensity of the saturated spectrum.

One of the most important parameter for STD NMR is the saturation time used for the protein signals. During this period, polarization gets transferred from the protein to ligand due to cross-relaxation *via* intermolecular dipolar interaction. Quantification of the transferred saturation is further achieved by defining STD amplification factor (A_F) which is the fractional saturation received for the particular ligand proton and multiplied by a molar excess of the ligand over the protein [Cala and Krimm, 2015; Gairí et al., 2016; Meyer et al., 2004; Unione et al., 2014].

$$A_F = \frac{I_o - I_{sat}}{I_o} \times ligand\ excess \tag{2.3}$$

For amplification factor calculation, the ligand proton signal exhibiting the highest spectral integral value in the STD spectra is set to 100%, whereas all other proton signals are normalized with respect to this proton. To precisely map the ligand proximity to protein, STD build-up curves are generated by plotting the amplification factor against the saturation time used for protein signal saturation by using Eq.(2.4):

$$A_F = STD_{max}\left(1 - e^{-k_{sat}t}\right) \tag{2.4}$$

where STD_{max} and k are the maximum STD intensity and the observed saturation rate constant, respectively.

Furthermore, the dissociation constant (K_D) of the ligand-protein complex can also be extracted from the STD NMR experiments. Analysis of the amplification of the STD effect as a function of ligand concentration allows the extraction of the K_D using Eq(2.5) [Nobrega & Cabrita, 2011]

$$A_F = \frac{\alpha_{STD}[L]}{K_D + [L]} \tag{2.5}$$

where α_{STD} is the maximal amplification factor, K_D is the dissociation constant, and L is the ligand concentration. In the case of STD NMR, where [L]>>[P] and A_F will increase with the increase in ligand concentration until a maximum amplification (α_{STD}) is reached.

In the present thesis, Chapters 3 and 5 demonstrate the application of STD NMR for group epitope mapping (GEM) and binding affinity determination in the case of OP-BSA and OP-trypsin interaction. It should be pointed out here that there are number of molecular systems other than small molecule-protein such as carbohydrate-protein, small molecule-carbohydrate, small molecule-lipid, are reported in literature where STD experiments have been performed successfully for quantification of similar kinetic parameters [Angulo and Nieto, 2011; Assfalg et al., 2016; Balazs et al., 2013; Haselhorst et al , 2009; Johnson et al, 2003; Longstaffe et al, 2010; García et al, 2018; Vasile et al, 2018].

2.3.4 NMR Relaxation for Ligand-Protein Interaction Study

^{1}H spin-lattice relaxation measurements and analysis are the other possible effective NMR method employed for quantifying ligand-macromolecule interaction in solution. Relaxation analysis of the ligand protons in the presence of protein facilitates the understanding of the subtle changes in the relaxation behavior of the ligand during association/complexation due to alterations in the motional regimes accessed by the ligand. Measurement of non-selective (R_1^{NS}) and selective spin-lattice relaxation rates (R_1^{SE}) is a ligand-based NMR approach that allows one to investigate ligand binding to protein by analyzing the change in R_1^{NS} and R_1^{SE} values due to molecular interaction that results in the change in molecular rotational correlation time (τ_c) [He et al, 2016a; Li et al, 2007; Martini et al, 2008; Rossi et al, 2001]. In the present thesis, a brief principle of NMR R_1^{NS} and R_1^{SE} measured for the ligands have been discussed.

Figure 2.6 represents the standard Bruker pulse sequences based on inversion recovery experiment with water presaturation commonly used for relaxation measurements. The inversion of ligand proton signals is achieved either by employing a non-selective 180° pulse or by a selective 180° pulse to extract non-selective or selective spin-lattice relaxations rates, respectively.

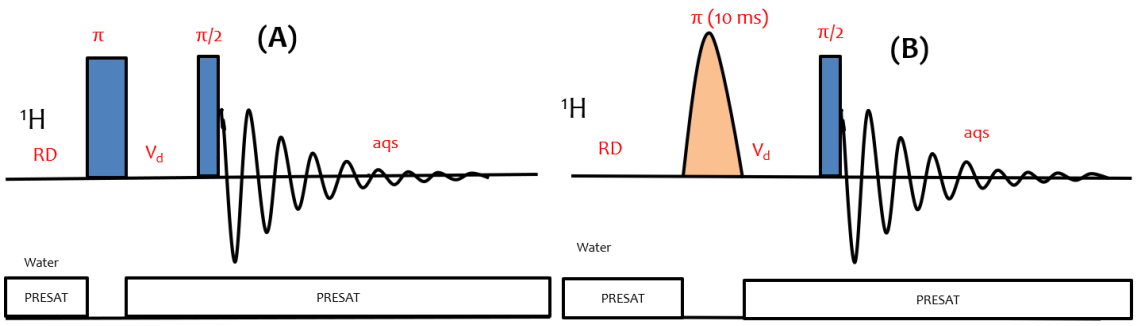

Figure 2.6 : Schematic drawing of NMR spin-lattice relaxation pulse sequence (A) non-selective spin-lattice relaxation (B) selective spin-lattice relaxation. RD: relaxation delay; Aqs: acquisition time; retangular blue bar: hard pulse; Brown Guassian shaped pulse: selective 180° pulse.

Eqs.(2.6-2.8) represents $R_1^{NS}$and R_1^{SE} in terms of auto-relaxation (ρ_{ij}) and cross-relaxation (σ_{ij}) rates considering intra and intermolecular dipolar interactions as the major relaxation mechanisms for the ligand protons in the solution in the presence of protein [Li et al, 2007; Martini et al, 2008].

$$R_1^{NS} = \sum_{i \neq j} \rho_{ij} + \sum_{i \neq j} \sigma_{ij} \quad (2.6)$$

$$R_1^{SE} = \sum_{i \neq j} \rho_{ij} \quad (2.7)$$

$$R_1^{NS} = R_1^{SE} + \sum_{i \neq j} \sigma_{ij} \quad (2.8)$$

The explicit form of $R_1^{NS}$and R_1^{SE} are further given by equations 2.9-2.10:

$$R_1^{NS} = \frac{1}{10}\frac{\gamma_H^4 \hbar^2}{r_{ij}^6}\left[\frac{3\tau_c}{1+\tau_c^2\omega_H^2} + \frac{12\tau_c}{1+4\omega_H^2\tau_c^2}\right] \quad (2.9)$$

$$R_1^{SE} = \frac{1}{10}\frac{\gamma_H^4 \hbar^2}{r_{ij}^6}\left[\frac{3\tau_c}{1+\tau_c^2\omega_H^2} + \frac{6\tau_c}{1+4\omega_H^2\tau_c^2} + \tau_c\right] \quad (2.10)$$

where $\hbar$ is reduced Plank's constant, γ_H and $\omega_H$are the proton magnetogyric ratio and Larmor frequency respectively, r_{ij} is the internuclear distance and τ_c is the molecular correlation time.

Eqs.(2.9) and (2.10) allow determination of molecular correlation time by using the experimentally measured ratio of $R_1^{NS}$and R_1^{SE} values for a particular proton using the relevant bond distance with the neighboring proton considering intramolecular dipolar interaction as the major relaxation mechanism [Reddy et al,2015; Reddy et al, 2018]. It must be noted here that for the free state of the ligand considering the fast motion regime ($\omega_H\tau_c \ll 1$), one may extract τ_c using Eq.(2.10) itself. Ligand-protein complex formation affects both $R_1^{NS}$and R_1^{SE}due to their dependence on the dynamic parameter τ_c. In case of fast molecular reorientation time or free ligand, the relation $R_1^{NS}>R_1^{SE}$ is satisfied as the system remains in extreme narrowing limit, *i.e.*, $\omega_H\tau_c \ll 1$, while in case of ligand-bound to protein, the relation $R_1^{NS} < R_1^{SE}$ holds good as the system moves to the slow motion regime, *i.e.*, $\omega_H\tau_c \gg 1$ exhibited by the macromolecules [Bonechi et al , 2011].

To extract the relevant kinetic parameters of the binding interaction, the ligand binding to a protein has been modeled as an equilibrium process as depicted in Eq.(2.11) exhibiting a fast chemical exchange between the bound and free state of the ligand.

$$M + L \leftrightarrow ML \quad (2.11)$$

where [M], [L] and [ML] are the molar concentration of the macromolecule, free ligand, and the complex, respectively with a thermodynamic equilibrium constant Kdefined as follows:

$$K = \frac{[ML]}{[M][L]} = \frac{[ML]}{\{[M_0]-[ML]\}[L]} \quad (2.12)$$

$$K[M_0][L] - K[ML][L] = [ML] \quad (2.13)$$

$$K[M_0][L] = [ML]\{K[L] + 1\} \quad (2.14)$$

$$[ML] = \frac{K[M_0][L]}{1+K[L]} \quad (2.15)$$

The binding parameters, namely the equilibrium constant, can be extracted from NMR experiments in case of a fast-chemical exchange condition between the bound and free state with respect to NMR relaxation timescale. For accurate quantitation, the total amount of bound ligand should be small compared to the free ligand, and also the ligand proton selective spin-relaxation rate must be strongly affected in the presence of protein [Bonechi et al, 1996]. In case of fast exchange between protein and free ligand, the R_{1obs}^{SE} (observed selective relaxation rate of the ligand protons) can be defined by Eq.(2.16) [He et al, 2016b; Martini et al, 2007; Yang et al, 2017; Zhai et al, 2018]:

$$R_{1obs}^{SE} = \chi_F R_{1F}^{SE} + \chi_B R_{1B}^{SE} \quad (2.16)$$

where R_{1obs}^{SE} is experimentally measured selective relaxation rate of the ligand protons in the presence of protein and is the weighted average of the selective spin-lattice relaxation rate of the bound state (R_{1B}^{SE}), and selective spin-lattice relaxation rate of the free state of the ligand (R_{1F}^{SE}) . χ_F and $\chi_B$are the fractions of the ligand in its free and bound state, respectively, with $\chi_F+\chi_B=1$. Eq.(2.16) can be rewritten as Eq.(2.17) by considering $\chi_B \ll 1$ and $R_{1B}^{SE} \gg R_{1F}^{SE}$ for the bound ligands [Fielding, 2007].

$$R_{1obs}^{SE} = R_{1F}^{SE} + \chi_B R_{1B}^{SE} \quad (2.17)$$

Further, Eq.(2.17) can be rearranged as Eq.(2.18) that can be further simplified in terms of Eq.(2.19).

$$R_{1obs}^{SE} - R_{1F}^{SE} = \chi_B R_{1B}^{SE} \quad (2.18)$$

$$\Delta R_1^{SE} = \chi_B R_{1B}^{SE} \quad (2.19)$$

In Eq.(2.19) the bound molar fraction χ_B can be given by Eq.(2.20):

$$\chi_B = \frac{[ML]}{[L]+[M]} \approx \frac{[ML]}{[L]} \quad (2.20)$$

Assuming that [L]>>[M], the bound molar fraction can be further represented as Eq.(2.21).

$$\chi_B = \frac{K[M_0]}{1+K[L]} \quad (2.21)$$

Finally, substituting Eq.(2.21) into (2.19), one may define the parameter affinity index of the ligand-protein complex using Eq.(2.22).

$$\Delta R_1^{SE} = \frac{K[M_0]}{1+K[L]} R_{1B}^{SE} = [\mathrm{A}]_{\mathrm{L}}^{\mathrm{T}}[\mathrm{M}] \quad (2.22)$$

where $\Delta R_1^{SE} = R_{1obs}^{SE} - R_{1F}^{SE}$ and [L] and [M] are the concentration of the ligand and protein, respectively [Rossi et al, 2001]. The plot of ΔR_1^{SE} against [M] gives straight line passing through origin with a slope that is equated to the affinity index $[\mathrm{A}]_{\mathrm{L}}^{\mathrm{T}}$. The affinity index is further used to calculate the global binding affinity of the ligand with the protein [Martini et al, 2006]. The major advantage of using affinity index $[\mathrm{A}]_{\mathrm{L}}^{\mathrm{T}}$ is that it reveals the strength of the specific and the non-specific interactions and also portrays the dynamics of the ligand-macromolecule interaction process. Further, it does not depend on the intrinsic relaxation properties of any proton. Moreover, the calculation does not require any prior information about the stoichiometry of the interaction [Reddy et al., 2015]. The dimensions of $[A]_L^T$ are $M^{-1}s^{-1}$ and the superscript T and subscript L define temperature and ligand concentration at which the binding event takes place. The Eq.(2.22) can also be written as:

$$\frac{1}{\Delta R_1^{SE}} = \frac{1+K[L]}{KR_{1B}^{SE}[\mathrm{M}]} \quad (2.23)$$

It is understood from Eq.(2.23) that a plot of $1/\Delta R_1^{SE}$ versus the ligand concentration [L] should be linear. The dissociation constant (K_D) can be evaluated from the intercept while the relaxation rate of the bound ligand can be measured from the slope of the plot. The presence of segmental motion in different parts of a molecule influences the selective relaxation rate by modulating the dipolar interaction among different protons. Therefore to remove the effect of different dynamical behavior arising from the different parts of a molecule on selective relaxation rate, ΔR_1^{SE} needs to be normalized using the relaxation rate of the free ligand [Reddy et al., 2015, 2018]. $[A]_L^T$ is then normalized to the relaxation rate of the free ligand and defined as the '*normalized affinity index*' $[A_N]_L^T$ (M^{-1}) as calculated by Eq.(2.24):

$$\Delta \mathrm{R}_{1\mathrm{N}}^{\mathrm{SE}} = \frac{K\mathrm{R}_{1\mathrm{B}}^{\mathrm{SE}}}{(1+K[\mathrm{L}])\mathrm{R}_{1\mathrm{F}}^{\mathrm{SE}}}[\mathrm{M}] = [\mathrm{A}_{\mathrm{N}}]_{\mathrm{L}}^{\mathrm{T}}[\mathrm{M}] \quad (2.24)$$

where $\Delta \mathrm{R}_{1\mathrm{N}}^{\mathrm{SE}} = \frac{\mathrm{R}_{1\mathrm{obs}}^{\mathrm{SE}} \mathrm{R}_{1\mathrm{F}}^{\mathrm{SE}}}{\mathrm{R}_{1\mathrm{F}}^{\mathrm{SE}}} = \frac{\Delta \mathrm{R}_1^{\mathrm{SE}}}{\mathrm{R}_{1\mathrm{F}}^{\mathrm{SE}}}$

Normalization of the affinity index is necessary to remove the effect of differential motional dynamics present in a small ligand giving rise to different segmental correlation times. [Martini et al, 2006; Wu et al, 2015].

2.4 COMPLEMENTARY METHODS

The NMR experimental findings reported in the present thesis have been further supported by computational methods and two other biophysical techniques, namely Isothermal Titration Calorimetry (ITC) and Fluorescence quenching analysis. In the following sections, a very brief description of these methods is provided.

2.4.1 Molecular Docking

Molecular docking (MD) is a computational method used as a complementary technique to NMR and provides an estimate of the binding event. MD is used to predict the binding modes and affinities of the ligand within the binding site of the particular target molecule [Meng et al, 2012]. The predictions of MD help to differentiate, optimize, and propose novel ligands. The 3D structure of the target is necessary to predict these interactions. In MD, thousands of possible poses of binding are examined and evaluated, and the best match for binding mode is predicted by the pose, which shows the lowest energy score. There are a number of docking software available, namely AutoDock [Morris et al, 1998], AutoDock Vina [Trott & Olson, 2010], FlexX [Rarey et al, 1996], FRED [Gasch and Stahl, 2003]. For the current thesis work discovery studio 4.0 is used to identify the binding interaction of OP-protein interaction.

2.4.2 Isothermal Titration Calorimetry

Isothermal Titration Calorimetry (ITC) offers the quantitative thermodynamic data pertaining to ligand-protein interaction and also provides information regarding the binding forces involved in the complex formation. Further, ITC alone can give direct information regarding the heat exchange as well as the binding constant of the complex. ITC is being considered as the 'golden standard' of ligand-protein interaction due to its reliable data, no need for modification of reporters, multiple output binding parameters, and broad target applicability [Kairys et al, 2019]. In the standard experimental setup, the changes in the heat absorption or heat release of the system are monitored when one of the binding partner is titrated into the solution of another binding partner, both with known concentrations, till the system attains equilibrium position [Du et al, 2016; Gasymov and Glasgow, 2007; Hawkes and Janata, 1973; Homans, 2007]. Ababou and Ladbury, 2006 describe the latest application and literature survey on ITC [Falconer & Collins, 2011]. The ligand-macromolecule kinetic study by ITC is described in various papers [Bundle and Sigurskjold, 1994; Callies and Daranas, 2016; Chaires, 2006; Fisher and Singh, 1995].

Due to the requirement of large amounts of protein, ITC is well suited for secondary screening. ITC experiments include: (a) the ligand titration into biomacromolecule solution, (b) measurement of heat absorbed or released during the ligand-protein binding process, (c) fitting of the raw data to evaluate binding affinity, thermodynamic parameters, and stoichiometry of complex.

2.6 FLUORESCENCE QUENCHING STUDY

Fluorescence spectroscopy is a non-destructive and widely used method to analyze ligand-protein interactions. Due to the higher signal-to-noise ratio, fluorescence is more sensitive than the absorption spectroscopy. The requirement of protein concentration is very small that can range between nanomolar (nm) to millimolar (mm) scale. The change in fluorescence intensity of a fluorophore occurs during molecular interaction with another molecule. In case fluorescence intensity reduces due to such interaction, it is known as quenching of fluorescence intensity. This can be induced either as a result of the formation of quencher-fluorophore complex or as a result of random collisions of both. The former is known as static quenching, while the latter is called dynamic quenching [Joseph R. Lakowicz, 2006]. Any structural or conformational changes and complex formation that a protein can undergo in the presence or in the absence of a foreign molecule can be investigated by monitoring quenching of its fluorescent amino acid constituents (tryptophan, tyrosine, and phenylalanine). Amongst these three amino acids, tryptophan (Trp) is the dominant source of intrinsic protein fluorescence [Vivian & Callis, 2001]. Particularly in the case of albumins, tyrosine, and tryptophan serve as the intrinsic natural probe to study fluorescence of the proteins [Sułkowska, 2002]. The differences in fluorescence anisotropy or

fluorescence polarization are also used for molecular interaction. The decrease in intensity is usually described by the well-known Stern-Volmer Equation as given by Eq.(2.25):

$$\frac{F_0}{F} = 1 + K_{SV}[Q] = 1 + K_q\tau_0[Q] \quad (2.25)$$

where F_0 and F: the fluorescence intensities of fluorophore in absence and in presence of quencher, respectively; [Q]: concentration of quencher; K_{sv} [L mol^{-1}]: the Stern-Volmer constant; K_q [L mol^{-1} s^{-1}]: the quenching rate constant for bimolecular quenching; τ_0 : the average fluorescence lifetime of the fluorophore without the quencher. A linear Stern-Volmer plot indicates either dynamic (collisional) or static (complex formation) quenching, whereas an upward (positive) curvature denotes the possibility of a combination of quenching processes occurring simultaneously and/or availability of multiple binding sites on the protein. On the other hand, a downward (negative) curvature indicates the presence of a different class of fluorophore populations. Further, to quantify binding parameters, *i.e.*, the binding constant (K_A) and the number of binding sites (n) Eq.(2.26) can be used.

$$\log\left[\frac{(F_o - F)}{F}\right] = logK_A + nlog[Q] \quad (2.26)$$

where F_o and F are the fluorescence intensities of protein in the absence and presence of the quencher, respectively, and Q is quencher concentration. The intercept represents the binding constant (K_A), and the slope represents the number of binding sites (n). In the following, a brief report of fluorescence quenching analysis has been provided to understand the effect of drug coadministration on the drug-BSA complex formation for a system of Paracetamol (PC)-BSA, and 5-Fluorouracil (5FU)-BSA. Such analysis finds its importance in literature as it allows the understanding of the effect of competitive or cooperative binding events (Figure 2.7). The study presented here shows the effect of 5-FU on binding efficiency of PC with BSA.

The fluorescence emission intensity of BSA reduced significantly in the presence of varying concentrations of both the drugs at 280 nm, as shown in Figure 2.7 (a), which clearly indicated that both tryptophan and tyrosine residues are participating in binding with the drugs.

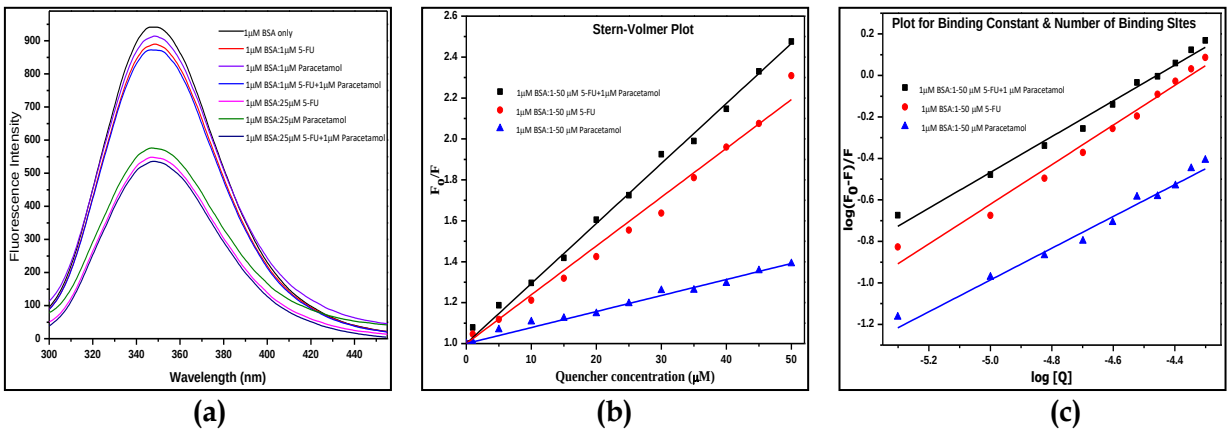

Figure 2.7 : (a) Fluorescence emission spectra (280 nm) of BSA (1 μM) with different concentration of 5FU and PC and effect of PC on binding of BSA-5FU, (b) Stern-Volmer plot for BSA-5FU, BSA-PC & BSA-5FU:PC, (c) The plot of log(F_o–F)/F versus log[Q].

Fluorescence quenching is determined by using the Stern-Volmer equation [Eftink & Ghiron, 1981] to determine K_{sv} by linear regression of a plot of F_0/F against $[Q]$. Further, the binding constant and the number of binding sites are calculated by Scatchard equation and

values for the same is given in Table 2.3 (Chinnathambi et al, 2014). A comparison of K_{sv}, $K_{A,}$ and n of the two drugs confirms that interaction between BSA-5FU is stronger than BSA-PC [Dahiya & Pal, 2018].

TABLE 2.3 : Fluorescence results for BSA-5FU, BSA-PC and BSA-PC:5FU complex.

Drugs	**Binding Constant (K_A) $\times 10^3$(L mol^{-1})**	**No. of Binding sites (n)**	**$K_{sv} \times 10^3$ L mol^{-1}**
BSA-PC	0.692±0.06 R^2=0.99	0.766	7.8±0.1 R^2=0.96
BSA-5FU	14.125±0.04 R^2=0.99	0.955	19.34±002 R^2=0.97
BSA-PC:5FU	7.021±0.04 R^2=0.99	0.862	13.8±0.06 R^2=0.96

The study demonstrates the applicability of fluorescence quenching analysis for the determination of binding parameters of PC-BSA and 5FU-BSA complexes.

…